Nanoscale

PAPER

View Article Online
View Journal | View Issue

Cite this: *Nanoscale*, 2022, **14**, 4188

Sustainable power generation *via* hydro-electrochemical effects†

Ahrum Sohn,[a] Yufan Zhang,[b] Anirban Chakraborty[a] and Choongho Yu *[a,b]

Received 24th November 2021,
Accepted 9th February 2022

DOI: 10.1039/d1nr07748a

rsc.li/nanoscale

Recent efforts towards energy scavenging with eco-friendly methods and abundant water look very promising for powering wearables and distributed electronics. However, the time duration of electricity generation is typically too short, and the current level is not sufficient to meet the required threshold for the proper operation of electronics despite the relatively large voltage. This work newly introduced an electrochemical method in combination with hydro-effects in order to extend the energy scavenging time and boost the current. Our device consists of corroded porous steel electrodes whose corrosion overpotential was lowered when the water concentration was increased and *vice versa*. Then a potential difference was created between two electrodes, generating electricity *via* the hydro-electrochemical method up to an open-circuit voltage of 750 mV and a short-circuit current of 90 μA cm^{-2}. Furthermore, electricity was continuously generated for more than 1500 minutes by slow water diffusion against gravity from the bottom electrode. Lastly, we demonstrated that our hydro-electrochemical power generators successfully operated electronics, showing the feasibility of offering electrical power for sufficiently long time periods in practice.

Introduction

Internet of things (IoT) and wearable devices have necessitated sustainable delivery of electrical power from the environment and/or wasted energy such as energy scavenging from solar energy, thermal energy, electrochemical energy, and mechanical energy.[1–4] Among them, water is an attractive energy source because it is abundant, low-cost, and environmentally benign without requiring particular weather, temperature, or vibration conditions for electrical energy generation.[5–10] The water-enabled energy conversion is a recently emerged field of study where the ion transport in an ion conductor (serving as an electrolyte) generates voltage between electrodes. The ion transport is governed by the diffusion of water molecules, which can be triggered by temperature difference[11–15] or concentration difference of water.[7,8,10,16–19] Various methods generating electricity from water including triboelectrification,[20–23] the streaming current,[24,25] the ion-gradient induced electric power generation[19,26] and the development of an interfacial structure[27,28] have been reported. When water diffusion is utilized, the generated voltage (~1 V) is adequate to operate small wearable electronic devices, compared to the tiny voltage from thermoelectrics[12,29] and large voltage from triboelectrics.[1,30,31] Nevertheless, the duration of water-enabled current generation is rather short (on the order of minutes), which makes the actual electrical energy insufficient to operate electronics for the desired time periods. For example, the electric power generation using water droplets based on triboelectric effects can generate a peak voltage of several volts and a peak current of several tens of μA cm^{-2} with a single droplet (30 μL), but the generated energy is only in nanojoules due to the extremely short energy generation time (milliseconds).[20,32,33] Xu *et al.* reported moisture-induced directional movement of protons upon exposure to different humid conditions, generating open-circuit voltage on the order of 0.8 V and short-circuit current on the order of 150 μA cm^{-2}, which are acceptable to operate electronics in practice.[17] However, the short discharging time (100 seconds) compared to the relatively long charging time (30 minutes) remains a challenge in addition to the unusually large change (70%) of relative humidity. Recently, Zhang *et al.* introduced a new concept of thermo-hydro-electrochemical energy scavenging by differentiating the electrochemical potential of two electrodes due to the thermally induced water migration.[34]

Here we employed hydro-electrochemical effects on corroded carbon steel electrodes. When the water concentration in one electrode is different from the other electrode, voltage and current were continuously obtained until the electrochemical potential difference between the two electrodes

[a]*Department of Mechanical Engineering, Texas A&M University, College Station, Texas 77843, USA. E-mail: chyu@tamu.edu*
[b]*Department of Materials Science and Engineering, Texas A&M University, College Station, Texas 77843, USA*

†Electronic supplementary information (ESI) available. See DOI: 10.1039/d1nr07748a

became identical. When water was in contact with the corroded steel electrodes, the corrosion overpotential decreased, resulting in the potential difference between the two electrodes. To maintain the potential difference for a longer period of time, the water diffusion was interrupted by embedding aligned chemically expanded graphite (CEG) perpendicular to the water transport direction in the interlayer. Upon supplying water to one of the electrodes, the maximum open-circuit voltage and short-circuit current of 0.8 V and 90 μA cm^{-2} were observed, respectively, and then they were gradually decreased over 1000 minutes. Finally, we demonstrated that our power generator could operate an electrochromic cell and a hygrometer.

Experimental

Our hydro-electrochemical cell is composed of two electrodes and one interlayer. For the electrode, carbon steel wool with a thickness of 300 μm (wire diameter: ~40 μm) was sandwiched between two carbon steel meshes (wire diameter: 230 μm; square hole dimension: 400 μm × 400 μm) by applying a pressure of 150 MPa. The dimension of the mesh was 2.5 cm × 1.5 cm with an active area of 1.5 cm × 1.5 cm by misaligning 1 cm from each side for electrical connection. Subsequently, 1 M HCl (500 μl) was dropped onto the electrodes to corrode the carbon steel, and then the sample was dried in a fume hood. The interlayer was fabricated by mixing an aqueous polystyrene sulfonic acid (PSS-H) solution (30% aqueous solution, Alfa Aesar) and chemically expanded graphite (CEG) using a pen-type sonicator (XL2000, Misonix Micron) with 100 W for 30 minutes. To synthesize the CEG, 10 g of graphite flakes (100 mesh, >99.9% purity) and 85 g of CrO_3 (>99% purity, Alfa Aesar) were added into 70 mL hydrochloric acid (37 wt%). Then the mixture was stirred at room temperature for 2 hours (using a magnetic stirrer bar). The solution was filtered using a vacuum filtration setup, and the collected flakes were washed with deionized water (washed multiple times using vacuum filtration) to obtain graphite intercalated with $H_2Cr_2O_7$.[35] The intercalated flakes were immersed in aqueous H_2O_2 (30% concentration) with a graphite concentration of 0.2 grams per 40 mL pure H_2O_2 for expansion by releasing gas (O_2 gas).[36] The expanded particles were collected and dried at room temperature overnight to obtain the CEG particles. The amount of CEG in 30 wt% PSS-H was set to 10 wt%. The CEG/PSS-H mixture solution (7.5 mL) was dropped into a container whose dimension was 20 mm × 20 mm × 2 mm. Under ambient conditions, the CEG/PSS-H solution was dried for 24 hours with a water uptake rate of ~30 wt%. The corroded electrodes and the CEG/PSS-H interlayer were assembled by applying a pressure of 500 Pa. The gel-like CEG/PSS-H smeared onto the porous electrodes played a role in holding them together. The thickness of the device was about 2 mm.

To operate the hydro-electrochemical energy generator, water (200 μL) was applied onto the top electrode dropwise with a rate of 100 μL per second. Alternatively, water was soaked from the bottom electrode of the generator, which allowed for generating electricity for a longer period of time with continuous water supply due to capillary action through hydrophilic cellulose from a water reservoir. The water was delivered to the generator at a rate of ~0.5 mL per hour. Voltage and current from the hydro-electrochemical generator were measured by connecting two digital multimeters (Keithley 2000) and by using a load resistor box (resistance range: 1 Ω to 10 MΩ).

Results and discussion

Our hydro-electrochemical cell consists of two identical carbon steel electrodes and an interlayer made of polystyrene sulfonic acid (PSS-H) and CEG, as illustrated in Fig. 1a. The electrode was fabricated by sandwiching carbon steel wool between two carbon steel meshes. The sandwiched structure with fine wires from the wool was intended to increase the surface contact area with water. To improve the electrical connection between the meshes and the wool, the sandwiched structure was compressed, as shown in the plane view (Fig. 1b) and cross-sectional view (Fig. 1c) using an optical microscope. In the cross-sectional image, fine wires from the wool are shown between mesh wires whose diameter is bigger. On the outer plane of the electrode, woven mesh wires in a checkered pattern are seen, and steel wool was well entangled with the mesh, ensuring many electrical contacts between them. To facilitate hydro-electrochemical energy generation from the carbon steel, the electrodes were corroded with a hydrochloric acid solution prior to integrating them with the interlayer, which was confirmed by the color change from a silvery to a reddish color (Fig. 1d). The interlayer was prepared by drop-casting an aqueous mixture solution containing PSS-H and CEG into a container (Fig. 1e). During the water evaporation process without disturbance, the CEG particles were aligned in the direction parallel to the electrode due to gravity, as illustrated in Fig. 1f and shown in the scanning electron microscopy (SEM) images (Fig. 1g and h). The cracks in PSS-H indicated by the arrows in Fig. 1g suggest the presence of water passages perpendicular to the CEG plane.[11] This implies that water transport was effectively retarded by the aligned CEG. When water droplet was applied to the top electrode, the difference between the water uptake rates of the top and bottom electrodes was maintained for a longer period of time, which extended the electricity generation, as explained in more details below.

The device with the two corroded steel electrodes and CEG-embedded PSSH film was tested as a function of time, as revealed in the images showing the open-circuit voltage (blue, left) and the short-circuit current (red, right) in Fig. 2a when 200 μl of water was dropped on the top side (1.5 × 1.5 cm^2) of the electrode (see the inset of Fig. 2a). On the corroded electrode, a β-FeOOH/Fe^{2+} redox couple was present[34] and electrons were drawn and donated between the two corroded electrode, showing the short-circuit current upon creating the

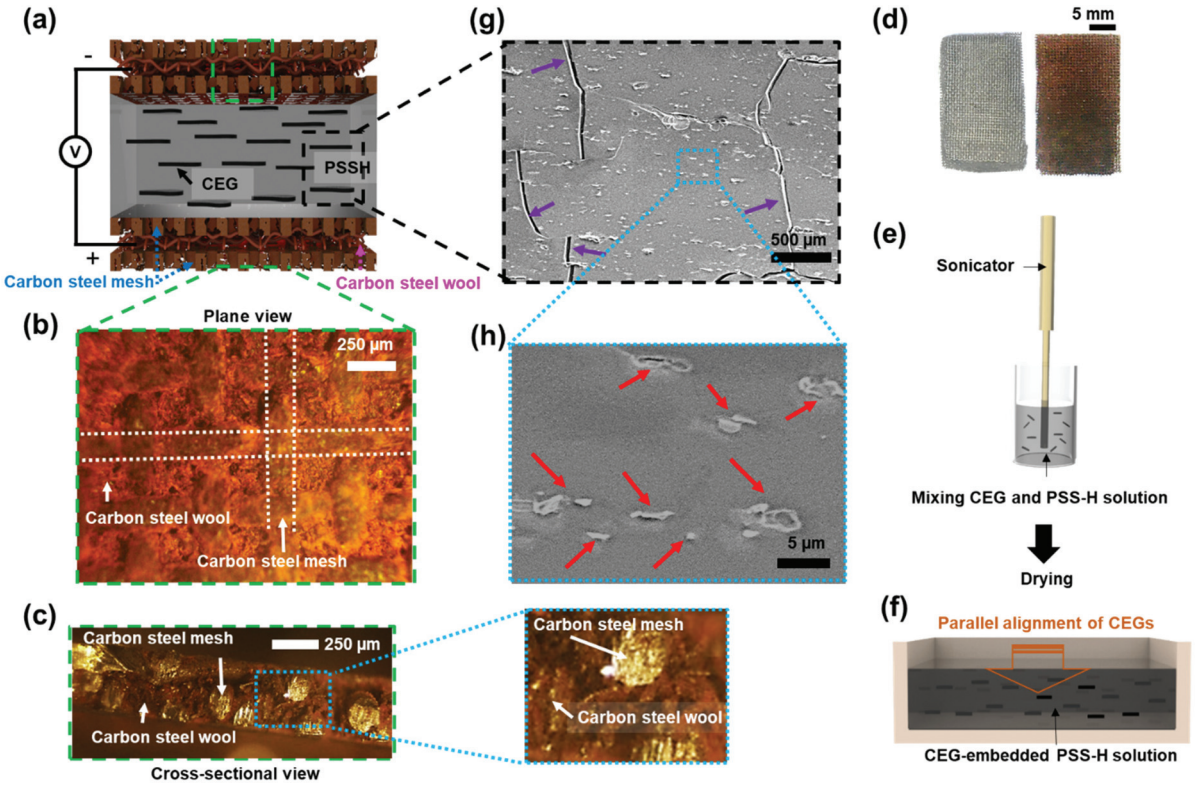

Fig. 1 (a) An illustration of our hydro-electrochemical device consisting of an interlayer made of CEG-embedded PSS-H and two identical corroded steel electrodes, where positive and negative terminals were connected for electrical measurements. Optical microscopy images showing (b) the outer surface of the electrode with interwoven mesh wires and wool in between, and (c) the cross-section of the electrode showing steel wool sandwiched with steel meshes. The white dashed lines indicate the boundary of the two mesh wires. (d) Images of the carbon steel mesh before (left side) and after (right side) corrosion. The interlayer was prepared by (e) dispersing CEG in the PSS-H solution using a sonicator and then (f) drying the mixture solution in a container without any disturbance so that CEG can self-align in a direction parallel to the bottom of the container. (g) A cross-sectional SEM image of the interlayer, where the cracks indicated by the purple arrows suggest water transport along the vertical direction. (h) A magnified image of 'g' showing aligned CEG embedded in PSS-H.

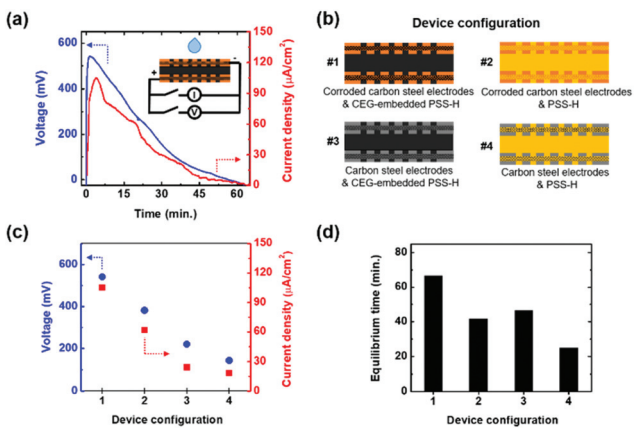

Fig. 2 (a) Open-circuit voltage (blue, left) and short-circuit current (red, right) of the hydro-electrochemical device as a function of time when water droplets were applied to the top electrode, as illustrated in the inset. (b) Four different electrode configurations (labeled as #1, #2, #3, and #4) of the device with corroded and pristine steel electrodes and PSS-H interlayers with and without CEG. (c) The maximum open-circuit voltage (blue, left) and short-circuit current (red, right) from the four different configurations shown in 'b'. (d) Elapsed time (called the equilibrium time) until the voltage reached zero for the four different devices in 'b'.

potential difference. When the water reached the interlayer made of non-porous and hygroscopic PSS-H, the water transport was driven by slow diffusion due to the concentration difference and gravity. Our device is advantageous in the operation as it works with a drop of water without necessitating special external stimuli or energy input. For instance, ion-gradient based electric power generation[19,26] requires spontaneous and continuous changes in relative humidity (over 70%) to generate a sufficient voltage. The maximum open-circuit voltage (~540 mV) and the maximum short-circuit current (~105 μA cm^{-2}) were observed at 4 minutes, and both voltage and current were gradually decreased over 65 minutes. The reductions can be attributed to the water diffusion from the top to the bottom due to the concentration difference and gravity. Eventually, the electrochemical potentials of both electrodes became identical, resulting in zero voltage and current when the water was distributed uniformly. To identify the role of each component in the device, we constructed four different configurations, as shown in Fig. 2b, by changing one component for each configuration. The #1 configuration is our main device with the CEG-embedded PSS-H interlayer and two identical corroded carbon steel electrodes. The #2 configur-

ation replaced the interlayer with pure PSS-H. The #3 configuration employed non-corroded steel electrodes, and #4 used the pure PSS-H interlayer with non-corroded steel electrodes. Fig. S1† shows the voltage and current from the four different devices as a function of time, and Fig. 2c presents the maximum open-circuit voltage (blue, left) and the maximum short-circuit current (red, right) for the four configurations. In addition, we measured the "equilibrium time" (Fig. 2d), which is the time period for the voltage to return to its initial value. The voltage became zero (initial value) when an equilibrium state in the water diffusion was reached in the interlayer. This equilibrium time is closely related to the duration of device operation after an initial event such as applying a water droplet. The #1 configuration displayed the highest voltage, current, and equilibrium time. The corroded electrodes (#1 and #2) displayed larger voltage and current compared with those of the non-corroded electrodes (#3 and #4), which were contributed by the water movement and proton transport.[11,34] In the same experiment with PSS-H as an interlayer and graphite as electrodes, voltage generation was only around 10 mV, as shown in Fig. S2.† This result is consistent with the outcomes in a paper revealing that the electrochemical effect generated larger voltages in an ion conductor with corroded electrodes.[34] The CEG (#1 and #3) extended the equilibrium time, extending the device operation time, indicating that the water diffusion was retarded. It is clear that the #1 configuration consisting of corroded steel electrodes and the CEG interlayer delivered the best performances.

We also noticed that CEG-embedded PSS-H resulted in higher output voltage than pure PSS-H. Fig. 3a and b illustrate the difference in the water diffusion with and without the CEG in the PSS-H layer. When water was applied to the top side of the device, the water diffused in the PSS-H layer toward the bottom due to gravity (Fig. 3a). On the other hand, water transport in the CEG-embedded PSS-H was effectively impeded by the CEG, so it takes longer for water to reach the bottom electrode (Fig. 3b). The pure PSS-H device generated a maximum open-circuit voltage of ~400 mV with an equilibrium time of 45 minutes (Fig. 3c), whereas the CEG increased the maximum open-circuit voltage to 540 mV and extended the equilibrium time over 60 minutes (Fig. 3d). Initially, before applying water to the top electrode, the electrochemical potentials of the two electrodes were identical (Fig. 3e). When water seeped into the top electrode, the electrode potential was lowered as a result of a smaller overpotential, as depicted in the Evans diagram.[34] The newly established oxidation line (the solid blue line in Fig. 3f) created a potential difference (*i.e.*, non-zero output voltage) between the top and bottom electrodes. At this stage, the voltage rapidly increased during the time period of 0 to approximately 5 minutes, as shown in Fig. 3c and d, because the electrode was very porous. As the water diffused all the way through the interlayer to the bottom electrode, the electrode potentials of the two electrodes were closer, showing a gradually decaying voltage. Therefore, the time duration of voltage generation strongly depends on the time period for water to reach the bottom electrode.

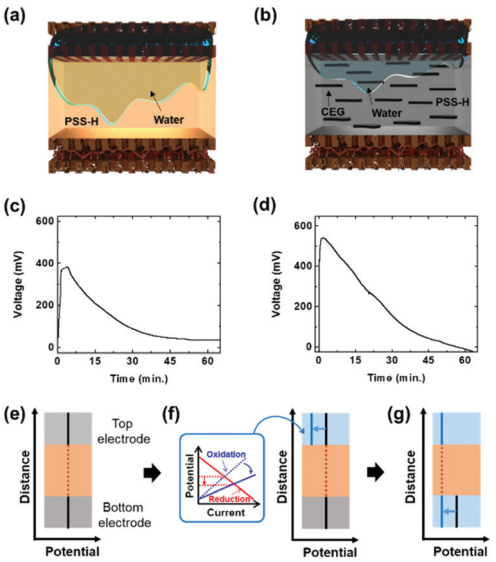

Fig. 3 Water diffusion from the top electrode to the bottom when (a) PSS-H and (b) CEG/PSS-H composites were used, illustrating that the CEG impeded the water diffusion due to its alignment perpendicular to the water diffusion path. Open-circuit voltage from the devices (c) without and (d) with CEG in the interlayer as a function of time after water droplets were applied to the top electrode. The electrochemical potential of the top and bottom electrodes (e) before and (f) after water was dropped on the top electrode. The water in the top electrode reduced the corrosion overpotential, creating the potential difference between the top and bottom electrodes, as illustrated in the Evans diagram with the newly established oxidation line (blue-solid line). (g) When the water diffused to the bottom electrode, the potential difference approached zero.

To have a more prolonged operation of the device, it is evident that dissimilar electrochemical potentials between the two electrodes should be maintained for a longer time period. Here we reversed the water diffusion direction from the bottom to the top by continuously supplying water from the bottom through a wet wipe (Kimwipes, Kimtech) from a water reservoir, as depicted in Fig. 4a. While water diffused from the bottom to the top due to the concentration difference in the interlayer, gravity pulled the water downward (Fig. 4b), and thereby water transport became sluggish, extending the time period for the water to diffuse all the way to the top electrode. According to the open-circuit voltage as a function of time (Fig. 4c), the maximum voltage went up to ~750 mV, which was higher than that in the previous case where the directions of water transport and gravity are coincident. The increase in voltage was observed for 60 minutes, compared to only ~4 minutes from the device shown in Fig. 3. Furthermore, the non-zero voltage was maintained for much longer, over 1000 minutes. The maximum short-circuit current was similar regardless of the water diffusion direction, but the non-zero current was observed for a much longer period of time, and maintained to be ~60 μA cm^{-2} even after 1500 minutes of operation (Fig. 4d). Such a long operation time is advantageous compared to other water based energy harvesters. For

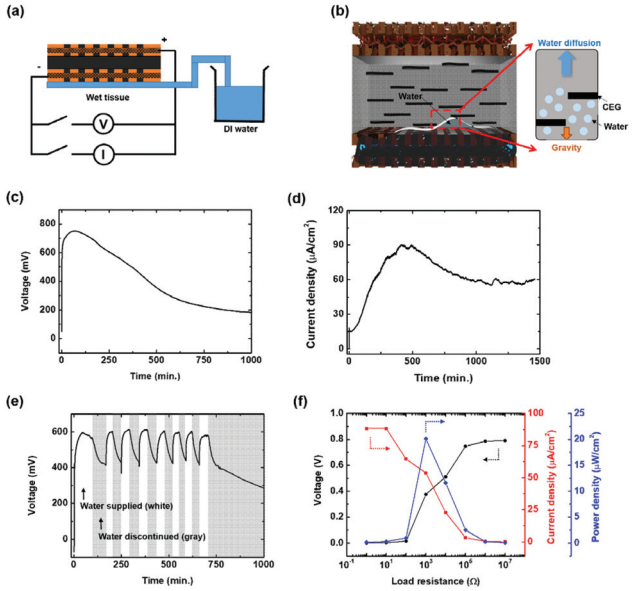

Fig. 4 (a) Water was continuously supplied from the bottom electrode through a wet tissue from a reservoir. (b) When water diffused from the bottom to the top, downward gravity and CEG impeded the diffusion speed. (c) Open-circuit voltage and (d) short-circuit current from the device with a continuous supply of water, and (e) open-circuit voltage when the water supply was intermittently discontinued. (f) Voltage (black), current (red), and power (blue) from the device as a function of load resistance.

example, triboelectric devices utilizing water droplets can generate several μA for short periods of time on the order of milliseconds in a form of alternating current that requires additional electronic components such as rectifiers and capacitors. Moreover, it is necessary to change the position of water droplets continuously to generate electricity.[20–22] On the other hand, the devices utilizing streaming current can generate voltage for several hours to a day, but the generated current is very small in the range between a few hundred nA and a few μA, which makes it difficult to continuously generate the desirable power of μW for operating electronics in practice.[24,25]

To verify the role of water, we supplied water to the bottom electrode and then discontinued to supply water repeatedly. Upon disconnecting the water supply (gray areas in Fig. 4e), the voltage dropped, and then it was recovered when water was resupplied. When water was not supplied, water diffused into the interlayer towards the top electrode, lessening the water concentration difference between the top and bottom electrodes and making the corrosion potentials of the two electrodes closer (*i.e.*, lower output voltage). We also measured the voltage and current as a function of external load resistance (1 Ω–10^7 Ω) in order to characterize device performances when they are under operation in practice. Fig. 4f shows the maximum voltage and areal current and the corresponding areal power output. With increasing resistance, the output voltage (black symbol) increased gradually, whereas the output current (red symbol) decreased. The output power (blue symbol) was obtained by multiplying the voltage and current, yielding a maximum power of 20 μW cm^{-2} with a load resistance of 10^3 Ω.

Finally, we have demonstrated that it is feasible to operate electronic devices such as an electrochromic display and a hygrometer. The electrochromic display changes color when charges are supplied because the redox states of the electrodes are altered. Fig. 5a shows the experimental setup for powering the display. Three power generators were connected in series to boost up the voltage, and water was supplied through wet wipes to the bottom electrodes of the generators. The voltage response as a function of time during the operation is shown in Fig. 5b. The corresponding electrochromic display when the electrochromic cell was connected to the power generator (red circle) is shown in the left inset of Fig. 5b. When the voltage reached 1.15 V after 800 s (blue circle), the pixel color of the display was altered, showing a different pattern (right inset of Fig. 5b). We also stored the harvested energy in a capacitor with four power generators connected in series. Fig. S3† shows the configuration of the setup with the hygrometer and four power generators. The recommended and minimum operation voltages for the hygrometer are 3 V and 1 V, respectively. Fig. 5c shows the voltage of the capacitor, whose capacitance is 470 μF when the four power generators were connected, and the inset depicts the corresponding electrical circuit diagram. After 150 seconds, the capacitor was charged to 1.5 V. When a hygrometer was connected to the charged capacitor, the hygrometer worked for 100 seconds as the output voltage of the capacitor decreased to the minimum voltage of 1 V (Fig. 5d).

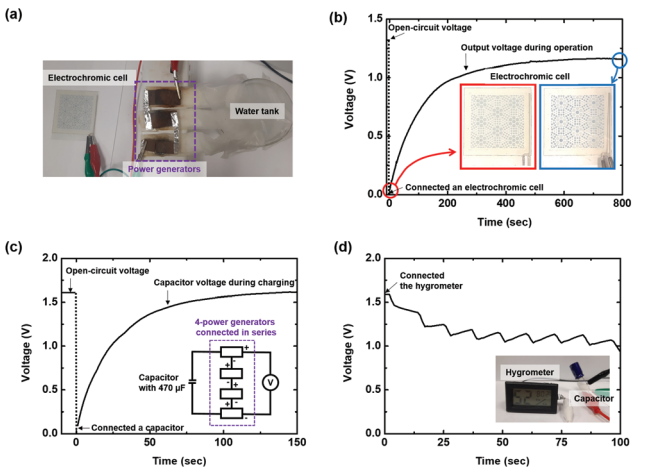

Fig. 5 (a) A photograph showing an electrochromic display powered by three serially connected hydro-electrochemical power generators. (b) Output voltage from the power generator in 'a', showing two different patterns in the electrochromic display right after the display was connected (red circle) and after 800 seconds (blue circle). (c) The voltage of a 470-μF capacitor charged by four serially connected hydro-electrochemical power generators. (d) The discharge voltage of the capacitor during the operation of the hygrometer.

Conclusions

This work offers a promising approach for extending the power generation time and boosting current by incorporating the corrosion potential difference caused by water diffusion. To facilitate the change in the corrosion potential by using water, the carbon steel electrodes were corroded and steel wool made of fine wires were used. The interlayer was made of hydroscopic PSS-H, where aligned CEG was embedded to impede the speed of water diffusion to maintain the potential difference between the top and bottom electrodes for a longer period of time. To identify the roles of the corroded steel and CEG, four different device configurations were tested, substantiating that the corroded steel and CEG gave rise to larger voltage and current as well as a longer operation time. When water was continuously supplied from the bottom against gravity, the water diffusion speed was lowered, resulting in a large open-circuit voltage of 750 mV and short-circuit current density of 90 μA cm^{-2} for over 1500 minutes, and a maximum power of 20 μW cm^{-2} with a load resistance of 10^3 Ω from a single device whose dimension was 1.5 cm by 1.5 cm. When four hydro-electrochemical power generators were connected in series, the output voltage was ~1.5 V, which is sufficiently large to operate electronics such as an electrochromic display and a hygrometer over 800 seconds. Our findings not only suggest a new approach *via* hydro-electrochemical effects to obtain outstanding performances with low-cost carbon steel but also provide opportunities to utilize various metal electrodes for further improving power generation.

Author contributions

A. S. conceived the idea, carried out the experiments and analyses, and wrote the paper. Y. Z. assisted the experiments. A. C. synthesized the chemically expanded graphite. C. Y. conceived the idea, supervised all the experiments and analyses, and reviewed and edited the manuscript.

Conflicts of interest

There are no conflicts to declare.

Acknowledgements

The authors acknowledge financial support from the US National Science Foundation (CBET 1805963).

References

1 R. Hinchet, H. J. Yoon, H. Ryu, M. K. Kim, E. K. Choi, D. S. Kim and S. W. Kim, *Science*, 2019, **365**, 491–494.
2 M. Jeong, I. W. Choi, E. M. Go, Y. Cho, M. Kim, B. Lee, S. Jeong, Y. Jo, H. W. Choi, J. Lee, J. H. Bae, S. K. Kwak, D. S. Kim and C. Yang, *Science*, 2020, **369**, 1615–1620.
3 B. Y. Yu, J. J. Duan, H. J. Cong, W. K. Xie, R. Liu, X. Y. Zhuang, H. Wang, B. Qi, M. Xu, Z. L. Wang and J. Zhou, *Science*, 2020, **370**, 342–346.
4 Z. H. Zhang, X. M. Li, J. Yin, Y. Xu, W. W. Fei, M. M. Xue, Q. Wang, J. X. Zhou and W. L. Guo, *Nat. Nanotechnol.*, 2018, **13**, 1109–1119.
5 S. S. He, Y. Y. Zhang, L. B. Qiu, L. S. Zhang, Y. Xie, J. Pan, P. N. Chen, B. J. Wang, X. J. Xu, Y. J. Hu, C. T. Dinh, P. De Luna, M. N. Banis, Z. Q. Wang, T. K. Sham, X. G. Gong, B. Zhang, H. S. Peng and E. H. Sargent, *Adv. Mater.*, 2018, **30**, 1707635 (1–7).
6 Y. X. Huang, H. H. Cheng and L. T. Qu, *ACS Mater. Lett.*, 2021, **3**, 193–209.
7 Y. Liang, F. Zhao, Z. H. Cheng, Y. X. Deng, Y. K. Xiao, H. H. Cheng, P. P. Zhang, Y. X. Huang, H. B. Shao and L. T. Qu, *Energy Environ. Sci.*, 2018, **11**, 1730–1735.
8 X. M. Liu, H. Y. Gao, J. E. Ward, X. R. Liu, B. Yin, T. D. Fu, J. H. Chen, D. R. Lovley and J. Yao, *Nature*, 2020, **578**, 550–554.
9 W. H. Xu, Y. X. Song, R. X. Xu and Z. K. Wang, *Adv. Mater. Interfaces*, 2021, **8**, 2000670 (1–19).
10 F. Zhao, L. X. Wang, Y. Zhao, L. T. Qu and L. M. Dai, *Adv. Mater.*, 2017, **29**, DOI: 10.1002/adma.201604972.
11 M. Jeong, J. Noh, M. Z. Islam, K. Kim, A. Sohn, W. Kim and C. Yu, *Adv. Funct. Mater.*, 2021, **31**, 2011016 (1–7).
12 S. L. Kim, K. Choi, A. Tazebay and C. Yu, *ACS Nano*, 2014, **8**, 2377–2386.
13 S. L. Kim, J. H. Hsu and C. Yu, *Org. Electron.*, 2018, **54**, 231–236.
14 S. L. Kim, J. H. Hsu and C. Yu, *Nano Energy*, 2018, **48**, 582–589.
15 A. M. A. Mageeth, S. Park, M. Jeong, W. Kim and C. Yu, *Appl. Energy*, 2020, **268**, 114975 (1–9).
16 S. Lee, J. Eun and S. Jeon, *Nano Energy*, 2020, **68**, 104364 (1–5).
17 T. Xu, X. T. Ding, Y. X. Huang, C. X. Shao, L. Song, X. Gao, Z. P. Zhang and L. T. Qu, *Energy Environ. Sci.*, 2019, **12**, 972–978.
18 F. Zhao, H. H. Cheng, Z. P. Zhang, L. Jiang and L. T. Qu, *Adv. Mater.*, 2015, **27**, 4351–4357.
19 F. Zhao, Y. Liang, H. H. Cheng, L. Jiang and L. T. Qu, *Energy Environ. Sci.*, 2016, **9**, 912–916.
20 Z. H. Lin, G. Cheng, S. Lee, K. C. Pradel and Z. L. Wang, *Adv. Mater.*, 2014, **26**, 4690–4696.
21 J. H. Nie, Z. M. Wang, Z. W. Ren, S. Y. Li, X. Y. Chen and Z. L. Wang, *Nat. Commun.*, 2019, **10**, 2264 (1–10).
22 X. L. Wei, Z. H. Zhao, C. G. Zhang, W. Yuan, Z. Y. Wu, J. Wang and Z. L. Wang, *ACS Nano*, 2021, **15**, 13200–13208.
23 W. Xu, H. Zheng, Y. Liu, X. Zhou, C. Zhang, Y. Song, X. Deng, M. Leung, Z. Yang, R. X. Xu, Z. L. Wang, X. C. Zeng and Z. Wang, *Nature*, 2020, **578**, 392–396.
24 B. Fan, A. Bhattacharya and P. R. Bandaru, *Nat. Commun.*, 2018, **9**, 4050 (1–7).

25 D. Z. Shen, M. Xiao, G. S. Zou, L. Liu, W. W. Duley and Y. N. Zhou, *Adv. Mater.*, 2018, **30**, 1705925 (1–8).
26 J. L. Xue, F. Zhao, C. G. Hu, Y. Zhao, H. X. Luo, L. M. Dai and L. T. Qu, *Adv. Funct. Mater.*, 2016, **26**, 8784–8792.
27 Y. S. Qin, Y. S. Wang, X. Y. Sun, Y. J. Li, H. Xu, Y. S. Tan, Y. Li, T. Song and B. Q. Sun, *Angew. Chem., Int. Ed.*, 2020, **59**, 10619–10625.
28 H. Y. Wang, Y. L. Sun, T. C. He, Y. X. Huang, H. H. Cheng, C. Li, D. Xie, P. F. Yang, Y. F. Zhang and L. T. Qu, *Nat. Nanotechnol.*, 2021, **16**, 811–819.
29 C. H. Yu, A. Murali, K. W. Choi and Y. Ryu, *Energy Environ. Sci.*, 2012, **5**, 9481–9486.
30 W. L. Liu, Z. Wang, G. Wang, G. L. Liu, J. Chen, X. J. Pu, Y. Xi, X. Wang, H. Y. Guo, C. G. Hu and Z. L. Wang, *Nat. Commun.*, 2019, **10**, 1426 (1–9).
31 A. Sohn, J. H. Lee, H. J. Yoon, H. H. Lee and S. W. Kim, *Nano Energy*, 2020, **74**, 104840 (1–7).
32 C. R. Liu, J. Sun, Y. Zhuang, J. Wei, J. Li, L. X. Dong, D. F. Yan, A. Hu, X. F. Zhou and Z. K. Wang, *Nanoscale*, 2018, **10**, 23164–23169.
33 W. H. Xu, X. F. Zhou, C. L. Hao, H. X. Zheng, Y. Liu, X. T. Yan, Z. B. Yang, M. Leung, X. C. Zeng, R. X. Xu and Z. K. Wang, *Natl. Sci. Rev.*, 2019, **6**, 540–550.
34 Y. F. Zhang, A. Sohn, A. Chakraborty and C. Yu, *Nat. Commun.*, 2021, **12**, 5269.
35 L. Dong, L. Zhang, S. Lin, Z. X. Chen, Y. N. Wang, X. X. Zhao, T. Q. Wu, J. J. Zhang, W. Liu, H. B. Lu and K. P. Loh, *Nano Energy*, 2020, **70**, 104482 (1–10).
36 S. Lin, L. Dong, J. J. Zhang and H. B. Lu, *Chem. Mater.*, 2016, **28**, 2138–2146.